

# Test of the cosmic distance duality relation for arbitrary spatial curvature

Jin Qin<sup>1\*</sup>, Fulvio Melia<sup>2†</sup> and Tong-Jie Zhang<sup>1‡</sup>

<sup>1</sup>*Department of Astronomy, Beijing Normal University, Beijing 100875, China*

<sup>2</sup>*Department of Physics, The Applied Math Program, and Department of Astronomy, The University of Arizona, AZ 85721, USA*

October 6, 2020

## ABSTRACT

The cosmic distance duality relation (CDDR),  $\eta(z) = (1+z)^2 d_A(z)/d_L(z) = 1$ , is one of the most fundamental and crucial formulae in cosmology. This relation couples the luminosity and angular diameter distances, two of the most often used measures of structure in the Universe. We here propose a new model-independent method to test this relation, using strong gravitational lensing (SGL) and the high-redshift quasar Hubble diagram reconstructed with a Bézier parametric fit. We carry out this test without pre-assuming a zero spatial curvature, adopting instead the value  $\Omega_K = 0.001 \pm 0.002$  optimized by *Planck* in order to improve the reliability of our result. We parametrize the CDDR using  $\eta(z) = 1 + \eta_0 z$ ,  $1 + \eta_1 z + \eta_2 z^2$  and  $1 + \eta_3 z/(1+z)$ , and consider both the SIS and non-SIS lens models for the strong lensing. Our best fit results are:  $\eta_0 = -0.021^{+0.068}_{-0.048}$ ,  $\eta_1 = -0.404^{+0.123}_{-0.090}$ ,  $\eta_2 = 0.106^{+0.028}_{-0.034}$ , and  $\eta_3 = -0.507^{+0.193}_{-0.133}$  for the SIS model, and  $\eta_0 = -0.109^{+0.044}_{-0.031}$  for the non-SIS model. The measured  $\eta(z)$ , based on the *Planck* parameter  $\Omega_K$ , is essentially consistent with the value ( $= 1$ ) expected if the CDDR were fully respected. For the sake of comparison, we also carry out the test for other values of  $\Omega_K$ , but find that deviations of spatial flatness beyond the *Planck* optimization are in even greater tension with the CDDR. Future measurements of SGL may improve the statistics and alter this result but, as of now, we conclude that the CDDR favours a flat Universe.

**Key words:** cosmological parameters, cosmology: observations, cosmology: theory, cosmic distance duality relation, strong gravitational lensing, high redshift quasars

## 1 INTRODUCTION

In cosmology, the luminosity distance,  $D_L$ , and angular diameter distance,  $D_A$ , are widely used measures for many astronomical observations. Etherington (Etherington 1933) first argued for a simple, yet profound, relationship between them,

$$\eta(z) \equiv \frac{D_A}{D_L} (1+z)^2 = 1, \quad (1)$$

often called the Etherington distance duality relation (DDR) (Etherington 2007), or the cosmic distance duality relation (CDDR). There are only three basic conditions required to make this relationship work:

1. The spacetime is described by a metric theory of gravity,
2. The photons travel along null geodesics,
3. The number of photons is conserved.

One may test the validity of the CDDR for any given cosmological model. An observed deviation from the CDDR may imply

some dramatic new physics. One should keep in mind, however, that unrecognized systematic uncertainties in the observations may also lead to a breakdown of the CDDR. It is therefore essential to select a means of testing the Etherington relation that is as accurate and reliable as possible.

An early attempt to validate the CDDR was presented by Bassett & Kunz (2004), who combined Type Ia SN data (SNe Ia) to measure  $D_L$ , and radio galaxies, compact radio sources and X-ray clusters to measure  $D_A$ . Several other early studies used a similar strategy to validate the CDDR based on the same types of data (Uzan et al. 2004; De Bernardis et al. 2006; Khedekar & Chakraborti 2011; Holanda et al. 2010; Li et al. 2011; Nair et al. 2011; Meng et al. 2012; Ellis et al. 2013). To obtain  $D_L$  and  $D_A$ , however, these investigations had to adopt a specific cosmological model, usually flat  $\Lambda$ CDM. But if the background model is incorrect, or imperfect, the result is less credible. More recent work has focused on testing the CDDR in a model-independent way (Liao et al. 2016; Lv & Xia 2016; Li & Lin 2018; Lin et al. 2018; Ruan et al. 2018; Lyu et al. 2020). Interestingly, none of these have indicated any significant violation of the CDDR within the margin of testing uncertainties. Nevertheless, all these works assumed a spatially flat cosmic background, so the conclusion inferred thus far may be biased.

\* E-mail: 201821160009@mail.bnu.edu.cn

† E-mail: fmelia@email.arizona.edu. John Woodruff Simpson Fellow

‡ E-mail: tjzhang@bnu.edu.cn

In this paper, we propose a new model-independent method to test the CDDR without assuming a spatially flat Universe. We use the recently released 161 galaxy-scale strong gravitational lensing (SGL) systems (Chen et al. 2019) to measure  $D_A$ . These are then combined with observations of high redshift quasars, which we use to infer  $D_L$  via a Bézier parametric fit, to test the CDDR at relatively high precision. Below, we shall describe both SIS and non-SIS lens models used for the SGL, along with an evaluation of their influence on various forms of parameterization for  $\eta(z)$ . To gauge the impact of spatial curvature on the CDDR, we test not only the *Planck* optimization of  $\Omega_K$  (Planck Collaboration et al. 2018), but also 20 other assumed values.

In § 2, we introduce the methodology we shall follow to test the CDDR for a Universe with arbitrary curvature. Then we describe the observations of SGL's and the reconstruction of the luminosity distance using high-redshift quasars in § 3. We present our results in § 4, and end with our conclusions in § 5.

## 2 METHODOLOGY

A homogeneous, isotropic expanding Universe can be characterized by the Friedmann-Lemaître-Robertson-Walker (FLRW) metric,

$$ds^2 = -c^2 dt^2 + a^2(t) \left( \frac{dr^2}{1 - Kr^2} + r^2 d\Omega^2 \right), \quad (2)$$

where  $a(t)$  is the scale factor,  $c$  is the speed of light, and the constant  $K$  represents the spatial curvature. Using Equation (2), we can define a dimensionless distance between the source at redshift  $z_s$  and the lens at  $z_l$  (Räsänen et al. 2015):

$$d(z_l, z_s) \equiv \frac{(1 + z_s)}{D_H} D_A(z_l, z_s), \quad (3)$$

where  $D_H \equiv c/H_0$ . Thus,

$$d(z_l, z_s) = \frac{1}{\sqrt{\Omega_K}} \sinh \left( \sqrt{\Omega_K} \int_{z_l}^{z_s} \frac{H_0}{H(z)} dz \right), \quad (4)$$

where  $D_A(z_l, z_s)$  is the angular diameter distance between  $z_s$  and  $z_l$ , and  $\Omega_K \equiv -K/H_0^2$  which, according to *Planck* (Planck Collaboration et al. 2018), is a small positive number. For convenience, we shall use the following notation:  $d_{ls} \equiv d(z_l, z_s)$ ,  $d_l \equiv d(0, z_l)$  and  $d_s \equiv d(0, z_s)$ .

Using Equation (4), the relationship between  $d_{ls}$ ,  $d_l$  and  $d_s$  may be written

$$d_{ls} = d_s \sqrt{1 + \Omega_K d_l^2} - d_l \sqrt{1 + \Omega_K d_s^2}, \quad (5)$$

which is usually referred to as the distance sum rule (Peebles 1993; Bernstein 2006; Räsänen et al. 2015). If the Universe has positive spatial curvature, as suggested by *Planck*, then the distance  $d_{ls}$  will be smaller than the difference between  $d_s$  and  $d_l$ .

To facilitate the use of strong lensing systems in order to find the angular diameter distance via Equation (5), we rewrite this equation as follows:

$$\frac{d_{ls}}{d_s} = \sqrt{1 + \Omega_K d_l^2} - \frac{d_l}{d_s} \sqrt{1 + \Omega_K d_s^2}, \quad (6)$$

where the ratio  $d_{ls}/d_s$  is extracted directly from the SGL's. Using the relations  $d_l = (1+z_l)D_A(0, z_l)/D_H$  and  $d_s = (1+z_s)D_A(0, z_s)/D_H$ , and expressing  $D_A(z_l, z_s)$ ,  $D_A(0, z_l)$  and  $D_A(0, z_s)$  as  $d_A^{ls} D_H$ ,  $d_A^l D_H$ ,

and  $d_A^s D_H$ , respectively, we then find from Equation (6) that

$$\begin{aligned} \frac{d_A^{ls}}{d_A^s} &= \sqrt{1 + \Omega_K (1 + z_l)^2 d_A^{l2}} \\ &\quad - \sqrt{1 + \Omega_K (1 + z_s)^2 d_A^{s2}} \frac{(1 + z_l) d_A^l}{(1 + z_s) d_A^s}. \end{aligned} \quad (7)$$

Note that  $d_A^{ls}$ ,  $d_A^l$  and  $d_A^s$  are dimensionless. Then, writing the CDDR as

$$\eta(z) = \frac{d_A}{d_L} (1 + z)^2, \quad (8)$$

we find that

$$\frac{d_A^{ls}}{d_A^s} \equiv \mathcal{R}(d_L^l, d_L^s, z_l, z_s) = K_l - \Phi K_s, \quad (9)$$

where

$$\Phi \equiv \frac{d_L^l \eta(z_l)(1 + z_s)}{d_L^s \eta(z_s)(1 + z_l)}, \quad (10a)$$

$$K_l \equiv \sqrt{1 + \left( \frac{d_L^l \eta(z_l)}{1 + z_l} \right)^2} \Omega_K, \quad (10b)$$

$$K_s \equiv \sqrt{1 + \left( \frac{d_L^s \eta(z_s)}{1 + z_s} \right)^2} \Omega_K. \quad (10c)$$

The quantities  $d_L^l$  and  $d_L^s$  are the dimensionless luminosity distance at  $z_l$  and  $z_s$ , respectively. In this paper, the ratio  $d_A^{ls}/d_A^s$  is obtained from the SGL's, while  $d_L^l$  and  $d_L^s$  are inferred from the quasar data.

We shall use three types of parameterization for  $\eta(z)$ :

$$\eta(z) = 1 + \eta_0 z, \quad (11a)$$

$$\eta(z) = 1 + \eta_1 z + \eta_2 z^2, \quad (11b)$$

$$\eta(z) = 1 + \eta_3 \frac{z}{1 + z}. \quad (11c)$$

Combining Equations (9) and (11a)–(11c), we may then optimize the CDDR by maximizing the likelihood function,

$$\mathcal{L} = \prod_{i=1}^n \frac{1}{\sqrt{2\pi} \sigma_i} \exp \left( - \frac{\left( \frac{d_A^{ls}}{d_A^s} / d_{A_i}^s - \mathcal{R}(d_{L_i}^l, d_{L_i}^s, z_{li}, z_{si}) \right)^2}{2\sigma_i^2} \right), \quad (12)$$

where  $n$  is the number of lenses,  $\mathcal{R}(d_{L_i}^l, d_{L_i}^s, z_{li}, z_{si})$  is given by Equation (9), and the variance can be written

$$\sigma_i^2 = \sigma_{int}^2 + \sigma_{A_i}^2 + \sigma_{\mathcal{R},i}^2. \quad (13)$$

In this expression,  $\sigma_{int}$  is the global intrinsic dispersion,  $\sigma_{A_i}$  is the measurement uncertainty in  $d_A^{ls}/d_A^s$ , and  $\sigma_{\mathcal{R},i}$  is the uncertainty in  $\mathcal{R}(d_{L_i}^l, d_{L_i}^s, z_{li}, z_{si})$ , which can be derived using an error propagation formula.

## 3 DATA

### 3.1 Angular Diameter Distance Obtained From SGL's

SGL's are widely used in constraining cosmic parameters, as well as testing the geometry of the universe. In general, there is a relationship between  $d_A^{ls}/d_A^s$  and parameters that characterize the SGL:

$$\frac{d_A^{ls}}{d_A^s} = \frac{c^2 \theta_E \mathcal{F}(\gamma, \delta, \beta)}{2 \sqrt{\pi} \sigma_0^2} \left( \frac{\theta_{\text{eff}}}{2\theta_E} \right)^{2-\gamma}, \quad (14)$$

where  $\theta_E$  is the Einstein radius and

$$\sigma_0 = \sigma_{ap} \left( \frac{\theta_{\text{eff}}}{2\theta_{ap}} \right)^\gamma \quad (15)$$

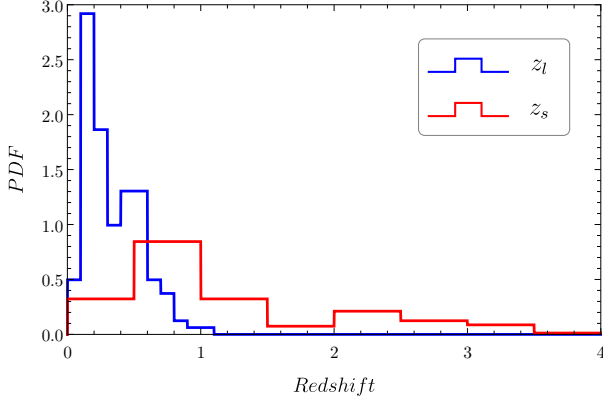


**Figure 1.** The redshift probability density histogram of lenses and sources for the 161 recently reported SGL’s (Chen et al. 2019).

is the velocity dispersion. This latter equation is known as the aperture correction formula, written in terms of the “aperture” velocity dispersion,  $\sigma_{ap}$ . Its value, and that of  $\theta_{eff}$ , may be found in Chen et al. (2019). As we shall see in Table 3.2 below, the “correction” index  $\nu$  is much smaller than 1. The function  $\mathcal{F}(\gamma, \delta, \beta)$  is defined as follows:

$$\mathcal{F}(\gamma, \delta, \beta) = \frac{\Gamma\left(\frac{\gamma}{2}\right)\Gamma\left(\frac{\delta}{2}\right)\Gamma\left(\frac{1}{2}(\gamma + \delta - 5)\right)}{2\Gamma\left(\frac{\gamma-1}{2}\right)\Gamma\left(\frac{\delta-3}{2}\right)\Gamma\left(\frac{\gamma+\delta}{2}\right)} \times \frac{-\beta(\gamma + \delta - 3) + \gamma + \delta - 2}{-2\beta + \gamma + \delta - 2}, \quad (16)$$

where  $\gamma$  is related to the total mass density,  $\delta$  is related to the luminosity density and  $\beta$  is the stellar orbital anisotropy (Chen et al. 2019; Lyu et al. 2020).

Combing this relation and the error propagation formula, we also obtain the uncertainty in the SGL measurements for the non-SIS model:

$$\sigma_A = \frac{d_A^{ls}}{d_A^s} \sqrt{(1-\gamma)^2 \left(\frac{\sigma_{\theta_E}}{\theta_E}\right)^2 + 4 \left(\frac{\sigma_{\sigma_0}}{\sigma_0}\right)^2}, \quad (17)$$

where  $\sigma_{\sigma_0}$  is the uncertainty in the velocity dispersion  $\sigma_0$ . In this paper we assume that  $\theta_E$  has a flat uncertainty of five percent, i.e.,  $\sigma_{\theta_E} = 0.05 \theta_E$ .

When using the singular isothermal sphere (SIS) model, i.e.  $\gamma = 2$ ,  $\delta = 2$ ,  $\beta = 0$ ,  $\mathcal{F}$  reduces to  $1/(2\sqrt{\pi})$  and Equation (14) simplifies to

$$\frac{d_A^{ls}}{d_A^s} = \frac{c^2 \theta_E}{4\pi \sigma_{SIS}^2}, \quad (18)$$

and the uncertainty is

$$\sigma_{A-SIS} = \frac{c^2 \theta_E}{4\pi \sigma_{SIS}^2} \sqrt{\left(\frac{\sigma_{\theta_E}}{\theta_E}\right)^2 + 4 \left(\frac{\sigma_{\sigma_{SIS}}}{\sigma_{SIS}}\right)^2}, \quad (19)$$

where  $\sigma_{SIS} \equiv f_e \sigma_0$ , and  $f_e$  corrects the deviation from  $\sigma_0$ . For the SIS model, intermediate-mass elliptical galaxies ( $200 \text{ km s}^{-1} < \sigma_{ap} \leq 300 \text{ km s}^{-1}$ ) are the most reliable for our test (Cao et al. 2016). For the non-SIS model, we use three subsamples (SLACS, S4TM, SL2S, totaling 121 quasars) to reduce the systematic errors, taken from 161 SGL systems (see fig. 1). The subsamples bias the SIS model slightly so, among the 161 SGL’s, we keep only those with the limit of  $\sigma_{ap}$  mentioned above, leaving 109 lenses for the SIS model.

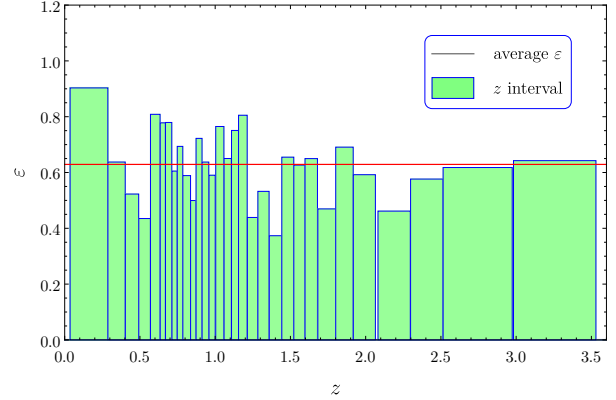


**Figure 2.** Determination of the slope  $\varepsilon$ . The width of each green rectangle is chosen to contain 50 quasars in that bin. Its height shows the best-fit  $\varepsilon$ -value at that redshift. The average  $\varepsilon$  value of all the subsamples is  $0.629 \pm 0.0873$ .

### 3.2 Luminosity Distance Obtained From High Redshift Quasars

Although Type Ia SNe are widely used standard candles to determine the luminosity distance, the limitations of these sources are now quite apparent. Their first disadvantage is observable events are restricted to redshifts  $\lesssim 2$  (Jones et al. 2013), so one cannot use them to measure  $D_L$  at high  $z$ . In addition, one must optimize several so-called “nuisance” parameters for their lightcurve simultaneously with other parameters in the specified cosmology. These “nuisance” parameters have very different values for different models, so the luminosity distance obtained from SNe is very model-dependent. A recently compiled high-quality catalog of high- $z$  quasars largely circumvents such problems (Risaliti & Lusso 2019).

Quasars are highly luminous objects visible at redshifts sometimes exceeding  $\sim 7$ . It has been known for several decades (see also Melia 2019) that their UV and X-ray emissions are correlated with a simple log-linear relation

$$\log(L_X) = \varepsilon \log(L_{UV}) + \alpha, \quad (20)$$

where  $L_X$  and  $L_{UV}$  are the rest-frame monochromatic luminosities at 2 keV and 2,500 Å, respectively, and  $\varepsilon$  and  $\alpha$  are two constants. In order to obtain the luminosity distance, we rewrite equation (20) as

$$\log_{10} D_L = \frac{1}{2(\varepsilon - 1)} (\log_{10} F_X - \varepsilon \log_{10} F_{UV} - \tilde{\alpha}), \quad (21)$$

where  $\tilde{\alpha} \equiv \alpha + (\varepsilon - 1) \log_{10} 4\pi$ . To fit the data more conveniently, we write the distance modulus as

$$\mu(z) = \frac{5}{2(\varepsilon - 1)} (\log_{10} F_X - \varepsilon \log_{10} F_{UV} - \tilde{\alpha}) + 5 \log_{10} \left( \frac{\text{cm}}{\text{Mpc}} \right) + 25. \quad (22)$$

We follow Risaliti & Lusso (2019) in finding the slope  $\varepsilon$  and the constant  $\tilde{\alpha}$ , though our approach is slightly modified. Risaliti & Lusso (2019) split the total quasar sample into subsamples located in narrow redshift bins, within which  $D_L$  in Equation (21) may be considered to be constant if the bins are sufficiently small. In that case, the fluxes  $F_X$  and  $F_{UV}$  will have a similar log-linear relation to that between  $L_X$  and  $L_{UV}$ . Risaliti & Lusso (2019) also found that the final value of  $\varepsilon$  is insensitive to the specified redshift bins as long as  $\Delta \log(z) < 0.1$ .

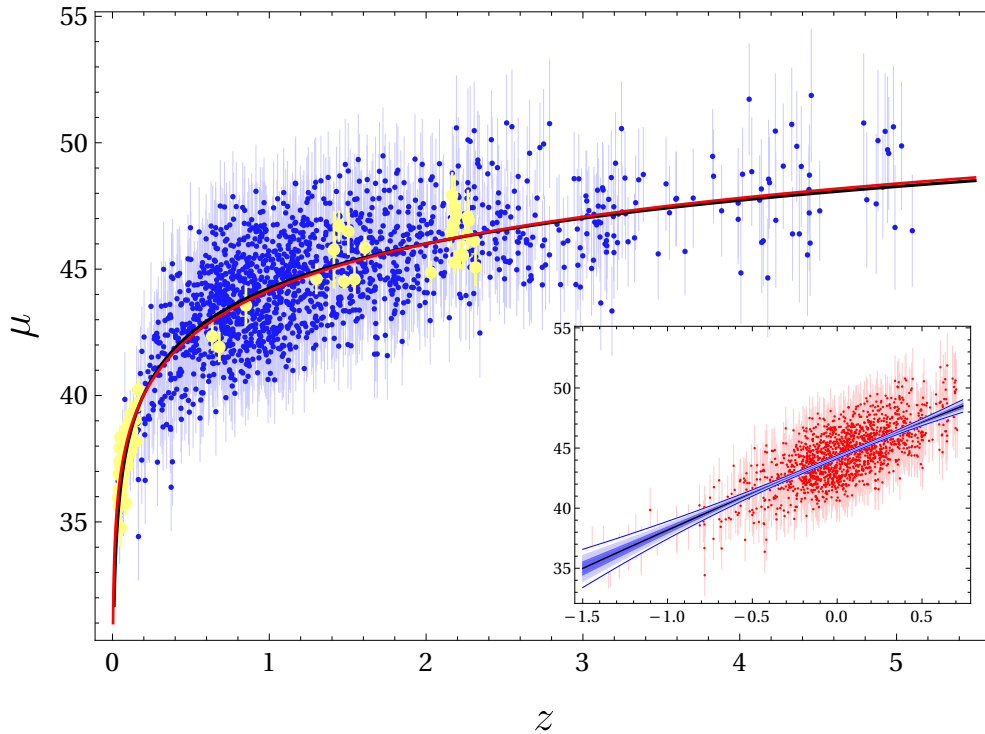


**Figure 3.** Distance modulus based on the [Risaliti & Lusso \(2019\)](#) quasar sample. The blue data with errorbars are calibrated quasars, while the yellow points represent the H<sub>II</sub> galaxy measurements. The red curve shows the *Planck*-optimized  $\Lambda$ CDM model, with  $\Omega_m = 0.315 \pm 0.007$  ([Planck Collaboration et al. 2018](#)). The black curve is the best-fit  $\mu(z)$  function, reconstructed with our Bézier method. The log subplot provides more detail concerning the Bézier fit, including the optimized curve and its  $3\text{-}\sigma$  uncertainty region.

**Table 1.** Best-fit parameters for all the models

Param.	SIS- $f_e$ 1	SIS- $f_e$ 2	SIS- $f_e$ 3	Non-SIS
$\eta_0$	$-0.021^{+0.068}_{-0.048}$	...	...	$-0.109^{+0.044}_{-0.031}$
$\eta_1$	...	$-0.404^{+0.123}_{-0.090}$	...	...
$\eta_2$	...	$0.106^{+0.028}_{-0.034}$	...	...
$\eta_3$	...	...	$-0.507^{+0.193}_{-0.133}$	...
$\nu$	$0.043^{+0.039}_{-0.039}$	$0.016^{+0.043}_{-0.044}$	$0.031^{+0.043}_{-0.044}$	$0.065^{+0.040}_{-0.039}$
$f_e$	$1.091^{+0.027}_{-0.026}$	$1.136^{+0.034}_{-0.032}$	$1.138^{+0.036}_{-0.034}$	...
$\gamma$	...	...	...	$1.883^{+0.089}_{-0.091}$
$\delta$	...	...	...	$1.917^{+0.506}_{-0.433}$
$\beta$	...	...	...	$-0.572^{+0.793}_{-0.506}$
$\sigma_{\text{int}}$	$\leq 0.048$	$\leq 0.046$	$\leq 0.047$	$0.069^{+0.021}_{-0.024}$

In this paper, we split the quasar sample using the following procedure. First, we sort all the quasars according to their redshift and make the first cut such that each subsample (except the last) contains 50 quasars. This procedure makes full use of the data in quasar-dense redshift bins and ensures a high-degree of accuracy. The best fit results for  $\varepsilon$ , from all the subsamples, are shown in Figure 2. We adopt the average value of all those individual subsample measurements, which equals  $0.629 \pm 0.0873$ . In earlier work, one of us ([Melia 2019](#)) used the same data set, though with alternative approaches to finding  $\varepsilon$ . The three models used to optimize these parameters in that work, including  $\Lambda$ CDM and the empirical cosmographic model, straddle the value of  $\varepsilon$  we have found here.

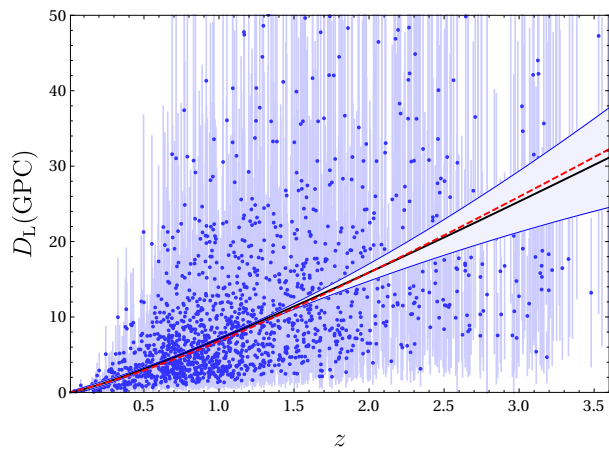


**Figure 4.** The luminosity distance calculated from the quasar data, and its  $1\sigma$  confidence region. The red dashed curve represents the theoretical luminosity distance predicted by  $\Lambda$ CDM with  $\Omega_m = 0.315$  and a spatial curvature constant  $\Omega_K = 0.001$  ([Planck Collaboration et al. 2018](#)). The theoretical curve lies well within the  $1\sigma$  confidence region.

To find  $\tilde{\alpha}$ , we use the same method developed by [Risaliti & Lusso \(2019\)](#), though calibrate the fits with H<sub>II</sub> galaxies rather than SNe. The luminosity ( $L_{\text{H}\beta}$ ) of Balmer lines from ionized hydrogen gas in these sources has a simple log-linear relationship with the velocity dispersion,  $\sigma_v$ , within the radiating plasma:

$$\log L_{\text{H}\beta} = \omega \log \sigma_v + \tau, \quad (23)$$

where  $\omega$  and  $\tau$  are two constants ([Melnick et al. 1987, 1988](#);

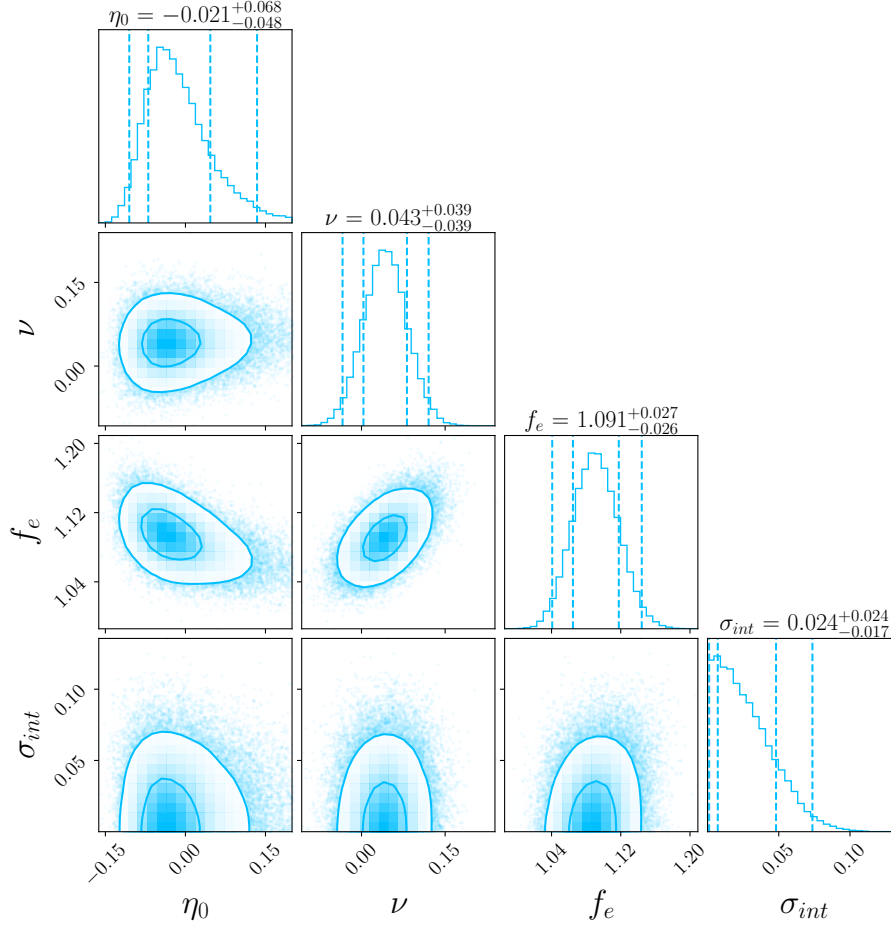


**Figure 5.** The 1D and 2D contours representing the  $1\sigma$  and  $2\sigma$  confidence regions for the parameterization  $\eta(z) = 1 + \eta_0 z$  using the SIS lens model.

Fuentes-Masip et al. 2000; Melnick et al. 2000; Bosch et al. 2002; Telles 2003; Siegel et al. 2005; Bordalo & Telles 2011; Plionis et al. 2011; Chávez et al. 2012, 2014; Mania & Ratra 2012; Terlevich et al. 2015). The distance modulus of an  $H_{\text{II}}$  galaxy can be written as

$$\mu_{H\beta} = -\tilde{\tau} + 2.5(\omega \log \sigma_v - \log F_{H\beta}) + 25 - 5 \log H_0, \quad (24)$$

where  $\tilde{\tau} = -2.5\tau - 5 \log H_0 + 125.2$  (Wei et al. 2016). Here  $H_0$  is the Hubble constant and we set  $H_0 = 67.35 \pm 16.47 \text{ km s}^{-1} \text{ Mpc}^{-1}$ , which is a model-independent value reconstructed by a machine learning method (Wang et al. 2020). In principle, the constants  $\omega$  and  $\tilde{\tau}$  should be constrained with a specified model. These constants have been shown to vary indistinguishably between different expansion scenarios, however, so Equation (24) is effectively model-independent (Wei et al. 2016; Ruan et al. 2018). This very weak dependence, if any, on the background cosmology is the principal reason we are opting to use  $H_{\text{II}}$  galaxies rather than SNe to calibrate the quasar sample. As described in the first paragraph of this section above, Type Ia supernovae cannot be used to infer a true model-independent distance modulus, since the parameters of the lightcurve must be optimized along with the model itself. Fortunately, the situation with  $H_{\text{II}}$  galaxies is very different, because their use thus far has shown that the constants in Equation (24) are very insensitive to the expansion rate. Following Ruan et al. (2018), we set  $\omega = 4.87^{+0.11}_{-0.08}$  and  $\tilde{\tau} = 32.42^{+0.42}_{-0.33}$  in this paper. By

cross-matching the  $H_{\text{II}}$  data with quasars in the overlapping redshift range (0.036, 2.315), we find an optimized value  $\tilde{\alpha} = 0.698$ .

Finally, we use a Bézier parametric fit to reconstruct the distance modulus,

$$\mu_n(z) = \sum_{d=0}^n \xi_d h_n^d(z), \quad (25)$$

where

$$h_n^d(z) \equiv \frac{n! (z/z_m)^d}{d!(n-d)!} \left(1 - \frac{z}{z_m}\right)^{n-d}, \quad (26)$$

in terms of the maximum redshift  $z_m$  in the quasar data, and positive coefficients  $\xi_d$ . This method was first developed by Amati et al. (2019) to reconstruct Hubble data and we use it here to reconstruct the continuous  $\mu(z)$  function. Following Wei & Melia (2020), we adopt  $n = 2$  to fit the discretized distance-modulus data. So the free parameters include:  $\beta_0, \beta_1, \beta_2$ , whose best-fit values are  $44.255 \pm 0.046, 59.258 \pm 0.354$  and  $69.118 \pm 6.575$ , respectively. The reconstructed  $\mu(z)$  function is shown in Figure 3.

Given the relationship between  $\mu(z)$  and  $D_L$ , we can directly obtain the dimensionless luminosity distance of quasars as

$$d_L = 10^{\mu(z)/5 - 5} / \text{Mpc}, \quad (27)$$

with a  $1\text{-}\sigma$  uncertainty

$$\sigma_{d_L} = \frac{\ln 10}{5} d_L \sigma_\mu. \quad (28)$$

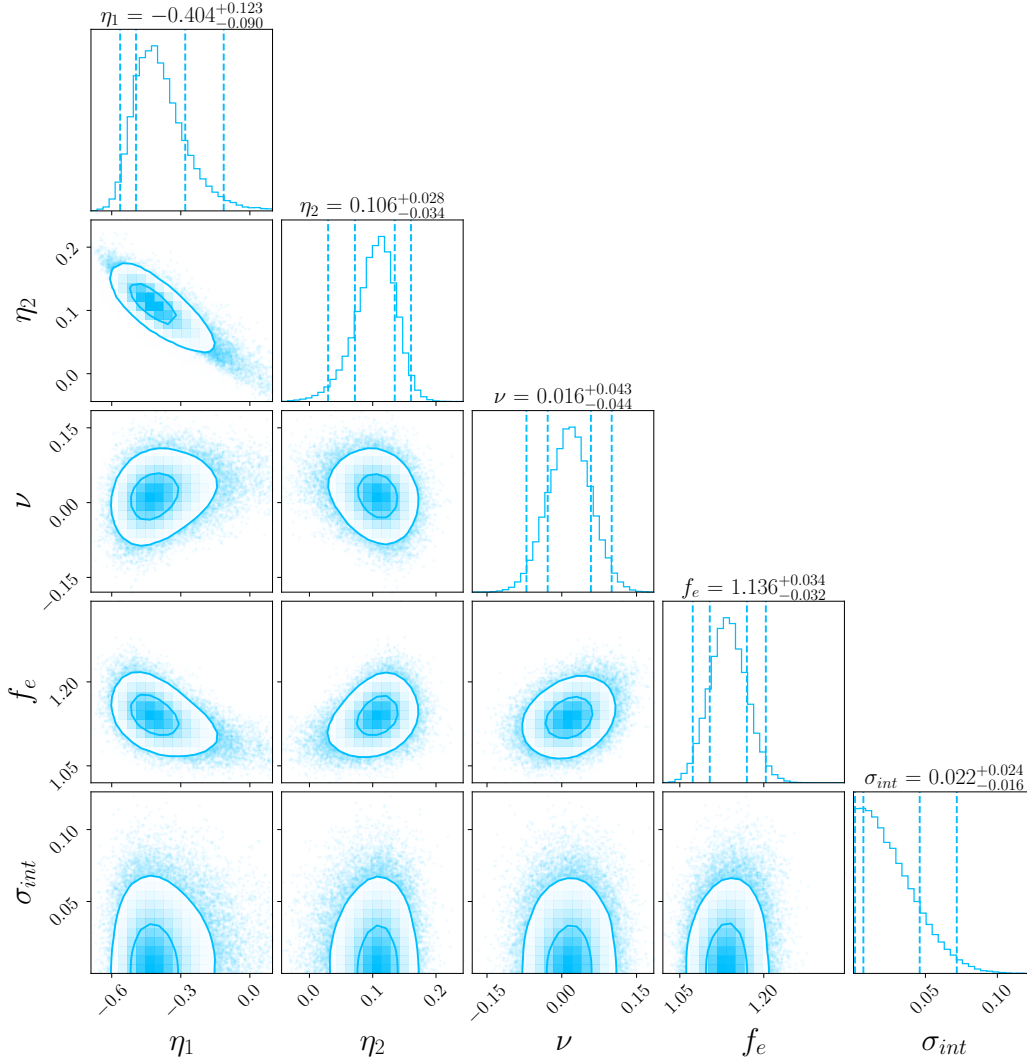


**Figure 6.** 1D and 2D contours representing the  $1\sigma$  and  $2\sigma$  confidence regions for the parameterization  $\eta(z) = 1 + \eta_1 z + \eta_2 z^2$  using the SIS lens model.

With the reconstructed luminosity distance, the uncertainty in  $\mathcal{R}(d_L^l, d_L^s, z_l, z_s)$  can be expressed as a function of  $d_L^l$ ,  $d_L^s$ ,  $\sigma_{d_L^l}^l$  and  $\sigma_{d_L^s}^s$ :

$$\sigma_{\mathcal{R}} = \sqrt{\left(K_l - \frac{1}{K_l} - \Phi K_s\right)^2 \left(\frac{\sigma_{d_L^l}^l}{d_L^l}\right)^2 + \left(\frac{\Phi}{K_s}\right)^2 \left(\frac{\sigma_{d_L^s}^s}{d_L^s}\right)^2}. \quad (29)$$

Note that  $K_l$  and  $K_s$  equal one if  $\Omega_K$  equals to zero, in which case Equation (29) simplifies to

$$\sigma_{\mathcal{R}} = \Phi \sqrt{\left(\frac{\sigma_{d_L^l}^l}{d_L^l}\right)^2 + \left(\frac{\sigma_{d_L^s}^s}{d_L^s}\right)^2}. \quad (30)$$

Equation (30) has been used in previous work similar to that reported here.

## 4 RESULTS AND DISCUSSION

### 4.1 The SIS model

In order to calculate the posterior distribution of the model parameters, we use the Python module `emcee`<sup>1</sup>, which is an Affine Invariant Markov chain Monte Carlo (MCMC) Ensemble sampler (Foreman-Mackey et al. 2013), to survey the posterior distribution in parameter space and to maximize the likelihood function in Equation (12). The resulting contour plots are made with the Python module `corner`<sup>2</sup> (Foreman-Mackey 2016).

We assumed the SIS lens model for the first application of the method described above. Combining the 109 SGL data with the  $d_L$  function reconstructed from the quasar measurements with the Bézier parametric method, we have found for the first parameterization  $\eta(z) = 1 + \eta_0 z$  that

$$\eta_0 = -0.021_{-0.048}^{+0.068}, \quad (31)$$

consistent with the CDDR to within  $1\sigma$  accuracy. Our  $1\sigma$  error

<sup>1</sup> <https://emcee.readthedocs.io/en/stable/>

<sup>2</sup> <https://corner.readthedocs.io/en/latest/>

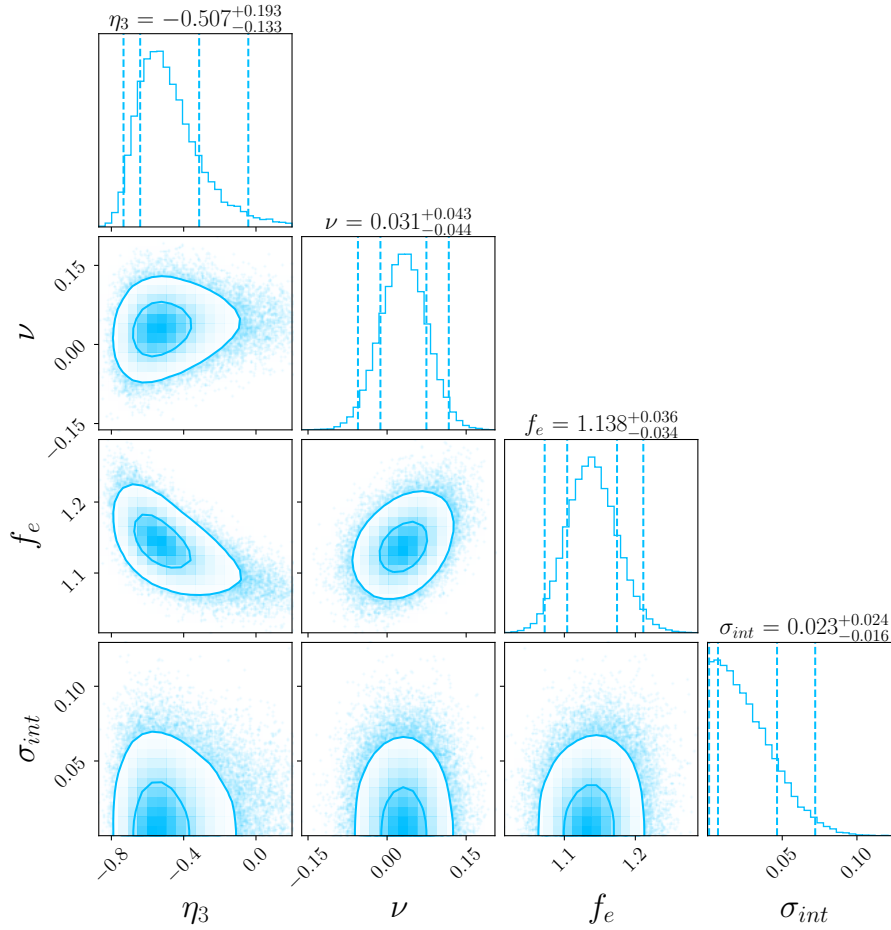


**Figure 7.** 1D and 2D contours representing the  $1\sigma$  and  $2\sigma$  confidence regions for the parameterization  $\eta(z) = 1 + \eta_3 z / (1 + z)$  using the SIS lens model.

is about half the size of that found by Lyu et al. (2020). Our result appears to favour a small negative value, however. The posterior distribution of  $\eta_0$ , and that of other related parameters, are plotted in Figure 5.

For the more complex parameterization  $\eta(z) = 1 + \eta_1 z + \eta_2 z^2$ , the best-fit parameter values are

$$\eta_1 = -0.404^{+0.123}_{-0.090} \text{ and } \eta_2 = 0.106^{+0.028}_{-0.034}, \quad (32)$$

and the corresponding contour plots are shown in Figure 6. This second-order parameterization, which was also used previously by Ruan et al. (2018), allows for greater precision. The  $1\text{-}\sigma$  errors in Equation (32) are smaller than those found by Ruan et al. (2018), a result stemming from the improved capability of the Bézier method, as well as an increase in the SGL sample size.

Finally, we have found for the third parameterization the optimized parameter value

$$\eta_3 = -0.507^{+0.193}_{-0.133}, \quad (33)$$

which disfavors zero by about  $3\sigma$ . This type of parameterization is more sensitive, so it appears to deviate from zero more robustly than the first parameterization. The corresponding contour plots are shown in Figure 7, and a summary of these results may be found in Table 3.2.

## 4.2 The non-SIS model

For the non-SIS lens model, we focus solely on the parameterization  $\eta(z) = 1 + \eta_0 z$  to avoid possible degeneracies among the larger number of free parameters (see Table 3.2). As it turns out, the result in this case is even stronger than that found for the SIS models, so the outcome is quite robust. The 1D and 2D marginalized distributions for  $\eta_0$  and the non-SIS parameters  $\gamma$ ,  $\delta$ ,  $\beta$ , etc. are shown in Figure 8. Specifically, the  $1\sigma$  confidence limits are:

$$\begin{aligned} \eta_0 &= -0.109^{+0.044}_{-0.031} \\ \gamma &= 1.883^{+0.089}_{-0.091} \quad \delta = 1.917^{+0.506}_{-0.433} \quad \beta = -0.572^{+0.793}_{-0.506} \end{aligned} \quad (34)$$

The non-SIS result for  $\eta_0$  is even more precise than that of the SIS models, at least based on the estimated errors. We have found that a zero value of  $\eta_0$  is excluded at a confidence level  $\sim 3\sigma$ . As was the case for the SIS model, this constraint on  $\eta_0$  favours a small negative correction to the CDDR, based on the *Planck*-optimized  $\Omega_K$  value. The remaining parameters in the non-SIS model are also optimized with high precision, with  $\delta$  and  $\beta$  consistent with their SIS values to within  $1\sigma$ .

## 4.3 The CDDR for more extreme deviations of $\Omega_K$ from zero

Although our focus thus far has been on the *Planck*-optimized value of  $\Omega_K$ , our CDDR test may be applied to any other choice of  $\Omega_K$ . It is beyond the scope of the present paper, however, to thoroughly

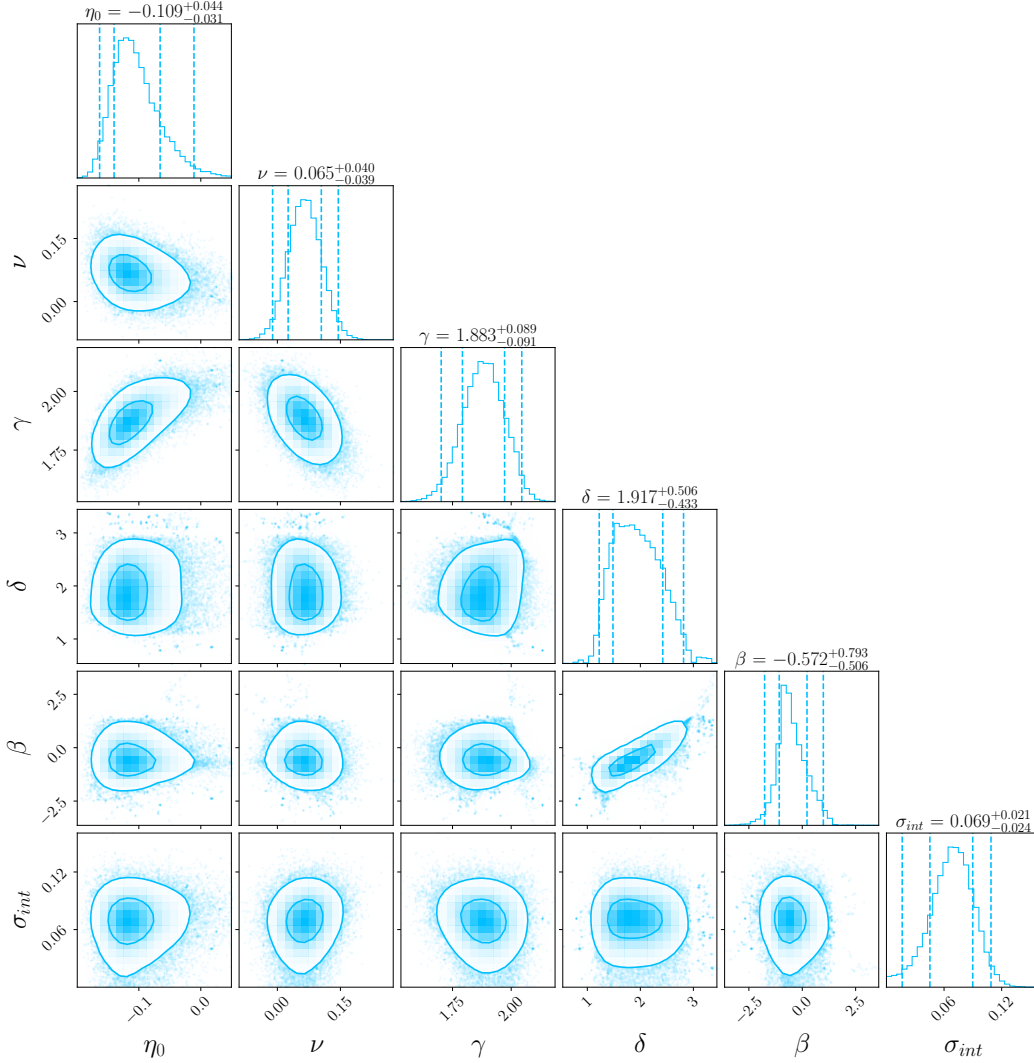


**Figure 8.** 1D and 2D contours representing the  $1\sigma$  and  $2\sigma$  confidence regions for the parameterization  $\eta(z) = 1 + \eta_0 z$  using a non-SIS lens model.

search parameter space in order to find an optimized value of  $\Omega_K$  different from that found by *Planck*. Here, we demonstrate the outcome for the CDDR, based on a broad sample of  $\Omega_K$  values.

Generally speaking, the distance sum rule in Equation (5) is invalid for  $\Omega_K < 0$  (Hogg 1999). We thus choose 20 positive  $\Omega_K$  values and repeat the above calculation using the SIS model with the parameterization  $1 + \eta_0 z$ . The test results are shown in Figure 9, which clearly shows that the CDDR strongly favours an  $\Omega_K$  near zero. Based on this limited survey, however, the value of  $\Omega_K$  consistent with the CDDR is actually somewhat positive, larger than that found by *Planck*. Though this is not yet strong evidence of a departure from the CDDR, the combination of results from *Planck* and our brief survey with other values of  $\Omega_K$  is intriguing enough to warrant future consideration as the data continue to improve.

#### 4.4 Possible factors that may bias the CDDR results

We have made several efforts in this work to ensure that the results are reliable and robust. Nevertheless, there may still be other factors biasing our conclusions that could be fixed with improved future observations, notably the SGL measurements. As noted, the

SGL dataset used in this paper was assembled from six subsamples, each of which has its own set of systematic errors. Therefore, our results may be biased due to possible inconsistencies in the SGL data. Unfortunately, we cannot rely on only one subset, since the greatly reduced number of sources would imply even bigger errors. In previous work similar to ours, Lyu et al. (2020) also pointed out this issue and found that the CDDR tends to negative values.

In addition to this, there may be a possibility that an incorrect choice of  $\Omega_K$  may be biasing the CDDR, but we cannot yet present a model-independent way of testing the value of  $\Omega_K$  on its own. One needs to keep in mind that many previous model-independent tests of  $\Omega_K$  were based on the assumption that the CDDR is valid. Of course, any model-independent and CDDR-independent test of  $\Omega_K$  would provide more robust conclusions regarding the CDDR itself. Looking to the future, our high-precision method of testing the CDDR should make deviations from Equation (1) more obvious if the spatial curvature in the real Universe turns out to be different from zero.



## 5 CONCLUSION

In this paper, we have demonstrated that the CDDR may be tested in a model-independent way by combining the luminosity distance inferred from high-redshift quasars with the angular diameter distance obtained from SGL's. This approach avoids potential difficulties faced by previously used methodologies based on Type Ia SNe. It is widely known that one needs to assume a specific cosmological model when using SNe in order to optimize the so-called “nuisance” parameters, rendering all such approaches model-dependent. Under such circumstances, one could not rule out the possibility that a deviation of  $\eta_0$  from 0 is caused by the incorrect model, rather than the data themselves.

Fortunately, we now have a much broader array of cosmological measurements offering alternatives to the use of Type Ia SNe, avoiding possible weaknesses stemming from the need to pre-assume some particular model. In this paper, we have proposed one such method and, in addition, have advanced the analysis by another significant step, i.e., by avoiding the need to assume a spatially flat background. Instead, we have carried out our analysis for several different  $\Omega_K$  values, including the optimization  $\Omega_K = 0.001$  from *Planck* (Planck Collaboration et al. 2018).

Our analysis has benefitted from the use of the Bézier reconstruction technique which, as we have seen, produces a more precise optimization of model parameters. With the smaller errors found in our results, our analysis has shown that *Planck*- $\Lambda$ CDM (with  $\Omega_K = 0.001$ ) is somewhat valid with the CDDR, though a slightly negative correction is favoured by these data. This approach avoids the introduction of possible systematic errors associated with the cosmological models, so any possible violation of the CDDR would originate from the physics itself.

By carrying out our analysis without assuming zero spatial curvature, this approach has extended the range of previous CDDR tests. There exists an abundance of evidence suggesting that  $\Omega_K$  is probably zero, including the results from *Planck*, but we have allowed the widest possible range of outcomes by allowing a deviation from complete spatial flatness. We have therefore probed the viability of the CDDR more generally, and have found that—at worst—any deviation of  $\Omega_K$  from zero consistent with the CDDR is much smaller than one. Nevertheless, the violation of the CDDR—should  $\Omega_K$  be consistent with the value found by *Planck*, or even slightly larger—represents some tension at the level of  $\sim 2\text{-}\sigma$  when using the parameterization  $\eta(z) = 1 + \eta_0 z$ .

Looking to the future, an increase in the number of SGL measurements would improve the precision of our approach even further. But already with the 161 data points at hand, combined with the Bézier method of reconstructing the luminosity distance, we have reduced the errors found in Ruan et al. (2018) by about a factor 1.5 for the SIS model, and a factor 3 – 4 for the non-SIS lens model. As the accuracy of such measurements continues to improve, we anticipate ruling out a non-flat cosmology with even greater confidence. Of course, the alternative could also be a clearer indication of a violation of the CDDR, requiring the introduction of new physics.

## ACKNOWLEDGMENTS

We are very grateful to the anonymous referee for comments that have led to a significant improvement of the analysis and presentation in this paper. FM is grateful to Amherst College for its support through a John Woodruff Simpson Lectureship. This work was

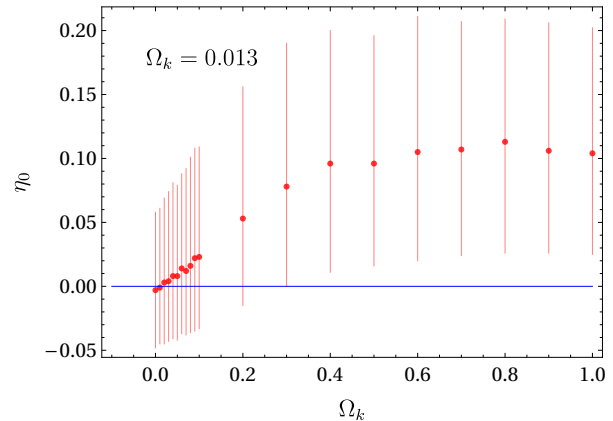


**Figure 9.** The relation between  $\eta_0$  and  $\Omega_K$  for a sample of spatial curvature values. A strict adherence to the CDDR, i.e.,  $\eta_0 = 0$ , is associated with  $\Omega_K = 0.013$ . The maximum deviation of  $\eta_0$  from one appears to be  $\sim 0.12$ .

partially supported by the National Science Foundation of China (Grant Nos. 11929301, 11573006) and the National Key R & D Program of China (2017YFA0402600).

## DATA AVAILABILITY STATEMENT

All of the SGL data can be taken from Chen et al. (2019) and the high-redshift quasar sample is available from the corresponding author of the paper by Risaliti & Lusso (2019). The  $H_{II}$  data used to calibrate the quasar distance modulus may be obtained from Wei et al. (2016).

## REFERENCES

- Amati, L., D’Agostino, R., Luongo, O., Muccino, M., & Tantalò, M. 2019, *MNRAS*, 486, L46
- Bassett, B. A., & Kunz, M. 2004, *PhRvD*, 69, 101305
- Bernstein, G. 2006, *ApJ*, 637, 598
- Bordalo, V., & Telles, E. 2011, *ApJ*, 735, 52
- Bosch, G., Terlevich, E., & Terlevich, R. 2002, *MNRAS*, 329, 481
- Cao, S., Biesiada, M., Yao, M., & Zhu, Z.-H. 2016, *Monthly Notices of the Royal Astronomical Society*, 461, 2192
- Chávez, R., Terlevich, E., Terlevich, R., et al. 2012, *MNRAS*, 425, L56
- Chávez, R., Terlevich, R., Terlevich, E., et al. 2014, *MNRAS*, 442, 3565
- Chen, Y., Li, R., Shu, Y., & Cao, X. 2019, *MNRAS*, 488, 3745
- De Bernardis, F., Giusarma, E., & Melchiorri, A. 2006, *IJMPD*, 15, 759
- Ellis, G. F. R., Poltis, R., Uzan, J.-P., & Weltman, A. 2013, *PhRvL*, 87, 103530
- Etherington, I. M. H. 1933, *Philosophical Magazine*, 15, 761
- . 2007, *General Relativity and Gravitation*, 39, 1055
- Foreman-Mackey, D. 2016, *The Journal of Open Source Software*, 1, 24
- Foreman-Mackey, D., Hogg, D. W., Lang, D., & Goodman, J. 2013, *Publications of the Astronomical Society of the Pacific*, 125, 306
- Fuentes-Masip, O., Muñoz-Tuñón, C., Castañeda, H. O., & Tenorio-Tagle, G. 2000, *ApJ*, 120, 752
- Hogg, D. W. 1999, arXiv e-prints, astro

- Holanda, R. F. L., Lima, J. A. S., & Ribeiro, M. B. 2010, *ApJL*, 722, L233
- Jones, D. O., Rodney, S. A., Riess, A. G., et al. 2013, *The Astrophysical Journal*, 768, 166
- Khedekar, S., & Chakraborti, S. 2011, *PhRvL*, 106, 221301
- Li, X., & Lin, H.-N. 2018, *MNRAS*, 474, 313
- Li, Z., Wu, P., & Yu, H. 2011, *ApJL*, 729, L14
- Liao, K., Li, Z., Cao, S., et al. 2016, *ApJ*, 822, 74
- Lin, H.-N., Li, M.-H., & Li, X. 2018, *MNRAS*, 480, 3117
- Lv, M.-Z., & Xia, J.-Q. 2016, *Physics of the Dark Universe*, 13, 139
- Lyu, M.-Z., Li, Z.-X., & Xia, J.-Q. 2020, *ApJ*, 888, 32
- Mania, D., & Ratra, B. 2012, *Physics Letters B*, 715, 9
- Melia, F. 2019, *MNRAS*, 489, 517
- Melnick, J., Moles, M., Terlevich, R., & Garcia-Pelayo, J.-M. 1987, *MNRAS*, 226, 849
- Melnick, J., Terlevich, R., & Moles, M. 1988, *MNRAS*, 235, 297
- Melnick, J., Terlevich, R., & Terlevich, E. 2000, *MNRAS*, 311, 629
- Meng, X.-L., Zhang, T.-J., Zhan, H., & Wang, X. 2012, *ApJ*, 745, 98
- Nair, R., Jhingan, S., & Jain, D. 2011, *JCAP*, 2011, 023
- Peebles, P. J. E. 1993, *Principles of physical cosmology* (Princeton university press)
- Planck Collaboration, Aghanim, N., Akrami, Y., et al. 2018, arXiv e-prints, [arXiv:1807.06209](https://arxiv.org/abs/1807.06209)
- Plionis, M., Terlevich, R., Basilakos, S., et al. 2011, *MNRAS*, 416, 2981
- Räsänen, S., Bolejko, K., & Finoguenov, A. 2015, *PhRvL*, 115, 101301
- Risaliti, G., & Lusso, E. 2019, *Nature Astronomy*, 3, 272
- Ruan, C.-Z., Melia, F., & Zhang, T.-J. 2018, *ApJ*, 866, 31
- Siegel, E. R., Guzmán, R., Gallego, J. P., Orduña López, M., & Rodríguez Hidalgo, P. 2005, *MNRAS*, 356, 1117
- Telles, E. 2003, in *Astronomical Society of the Pacific Conference Series*, Vol. 297, *Star Formation Through Time*, ed. E. Perez, R. M. Gonzalez Delgado, & G. Tenorio-Tagle, 143
- Terlevich, R., Terlevich, E., Melnick, J., et al. 2015, *MNRAS*, 451, 3001
- Uzan, J.-P., Aghanim, N., & Mellier, Y. 2004, *PhRvD*, 70, 083533
- Wang, G.-J., Ma, X.-J., & Xia, J.-Q. 2020, arXiv e-prints, [arXiv:2004.13913](https://arxiv.org/abs/2004.13913)
- Wei, J.-J., & Melia, F. 2020, *ApJ*, 888, 99
- Wei, J.-J., Wu, X.-F., & Melia, F. 2016, *MNRAS*, 463, 1144